Sensitivity to hole doping of Cu L_3 resonant spectroscopies: Inelastic x-ray scattering and photoemission of $La_{2-x}Sr_xCuO_4$

G. Ghiringhelli,[1] N. B. Brookes,[2] C. Dallera,[3] A. Tagliaferri,[4] and L. Braicovich[3]
[1]*CNR/INFM COHERENTIA and Dipartimento di Fisica, Politecnico di Milano, Piazza Leonardo da Vinci 32, 20133 Milano, Italy*
[2]*European Synchrotron Radiation Facility, B.P. 220, 38043 Grenoble Cédex, France*
[3]*CNR/INFM SOFT and Dipartimento di Fisica, Politecnico di Milano, Piazza Leonardo da Vinci 32, 20133 Milano, Italy*
[4]*CNISM and Dipartimento di Fisica, Politecnico di Milano, Piazza Leonardo da Vinci 32, 20133 Milano, Italy*
(Received 8 March 2007; revised manuscript received 19 July 2007; published 13 August 2007)

We present Cu L_3 edge resonant inelastic x-ray scattering (RIXS) and resonant x-ray photoemission spectroscopy (RXPS) of $La_{2-x}Sr_xCuO_4$ (x=0.0, 0.13, and 0.27). RIXS is found to be much more sensitive to the hole doping level than resonant photoemission. RIXS allows us to determine the average energy of *dd* excitations of both undoped and hole doped sites. The trade-off between the Raman and non-Raman spectral features depends on the doping level strongly in RIXS but weakly in RXPS. These experimental findings are consistently interpreted within a cluster model: The role of nonlocal core hole screening in the intermediate state is shown to be crucial. Nonlocal screening has an impact also on the interpretation of the L_3 x-ray absorption spectra in cuprates.

DOI: 10.1103/PhysRevB.76.085116 PACS number(s): 78.70.En, 71.70.Ch, 74.72.−h

I. INTRODUCTION

Resonant spectroscopies excited with x rays are very important in the study of strongly correlated solids mainly because of their intrinsic chemical and valence selectivity achieved by choosing the excitation energy. Two important approaches are resonant inelastic x-ray scattering (RIXS) and resonant x-ray photoemission spectroscopy (RXPS). The former is a photon-in photon-out method and is charge neutral,[1,2] whereas the latter is a photon-in electron-out technique,[3–6] so that it is an electron subtraction spectroscopy. It is thus interesting to compare the two approaches, at least in some significant cases. The high T_c cuprates hold a specific interest beyond their general importance because their *d*-to-*d* excitations can be directly studied with RIXS at the Cu L_3 edge.[7] *d*-to-*d* (or simply *dd*) excitations are transitions from the ground state to other electronic configurations characterized by a different distribution of the same number of electrons among the 3*d* derived levels. We will consider those excitations to have a localized character, as a consequence of the dominance of local electron-electron correlation with respect to hybridization and band formation. In Ref. 7, the excitation energy dependence of RIXS had not been studied. We address this topic here by studying both RIXS and RXPS vs the excitation energy $h\nu_{in}$. The comparison leads to interesting results despite some limitations set by the instrumental energy linewidth when working with ~930 eV photons. In fact, opposite to high resolution angle resolved ultraviolet photoemission,[8] Cu L_3 RIXS and RXPS cannot yet access the low energy scale. Nevertheless, we show in this article that, even on the eV energy scale, resonant spectra reveal evident changes in the electronic structure of cuprates when differently doped.

We have chosen $La_{2-x}Sr_xCuO_4$ (conventionally called LSCO) because it allows a direct control of the hole doping. We present RIXS and RXPS measurements taken on LSCO samples of very different doping levels and excited at a variety of energies across the Cu L_3 edge. We analyze three cases: the undoped compound La_2CuO_4 (conventionally called LCO), which is an antiferromagnetic insulator; one sample close to the optimal hole doping (x=0.13); and an overdoped sample near the boundary of superconductivity (x=0.27).[9] Our main finding is that the spectral function shows a much higher sensitivity to the doping in RIXS than in RXPS. RIXS has allowed us to determine the average energy of *dd* excitations in LSCO both in doped and undoped Cu sites. These results are important *per se* and pave the way to future more detailed RIXS experiments. Moreover, RIXS and RXPS appear to behave differently in the competition with the fluorescence and Auger signals, respectively. In fact, in all resonant spectroscopies, there are features bound to the incident photon energy (i.e., dispersive or Raman components) and features appearing at constant emitted energy (i.e., nondispersive or non-Raman). Non-Raman are the fluorescencelike contributions in photon emission (RIXS) and the ordinary Auger contributions in electron emission (RXPS). We show below that due to the different final state of the two processes, the non-Raman component is more sensitive to the doping in RIXS than in RXPS. Our phenomenological discussion is aimed at stimulating further experimental and theoretical research.

II. EXPERIMENTAL RESULTS: RESONANT INELASTIC X-RAY SCATTERING AND RESONANT X-RAY PHOTOEMISSION SPECTROSCOPY

The RIXS measurements were taken with the advances x-ray emission spectroscopy (AXES) spectrograph already used in Ref. 7, installed at the ID08 beamline of the European Synchrotron Radiation Facility (Grenoble, France) and equipped with a dedicated monochromator.[10,11] The scattering plane was horizontal and the incident linear polarization was vertical, perpendicular to the scattering plane. The combined energy resolution was set to 0.95 eV. A selection of the RIXS spectra is shown in Fig. 1: On the main peak,

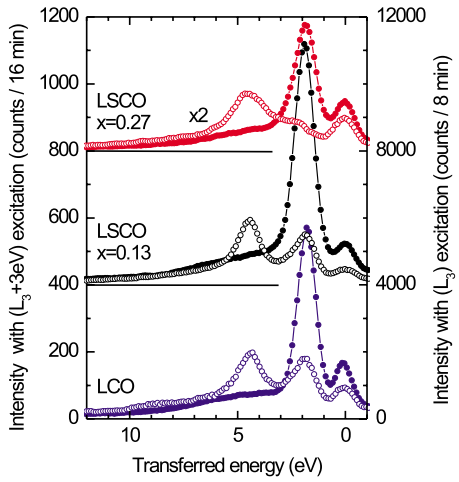

FIG. 1. (Color online) A selection of the RIXS spectra for the three samples. The full circles refer to the L_3 main peak excitation, and the open circles to the L_3+3 eV excitation. The spectra are as measured: one data point every 110 meV. For LCO and x=0.13, the accumulation time was 8 min at L_3 and 16 min at L_3+3 eV. For x=0.27, the accumulation time was doubled.

the count rate was approximately 130 counts/(s eV) [1.7 counts/(s eV)] for LCO and x=0.13 and 45 counts/(s eV) [0.8 counts/(s eV)] for x=0.27 at the L_3 (L_3+3 eV) excitation. The spectra were measured in a series of 2 min accumulations, and the total acquisition time varied between 8 and 32 min depending on the sample and excitation energy. The beamline Dragon monochromator was used in the RXPS measurements taken with a hemispherical Scienta 2002 photoelectron spectrometer. The combined energy resolution in RXPS was set to 0.35 eV. The count rate on the main peak was approximately 120 000 counts/(s eV) [14 000 counts/(s eV)] for all samples at the L_3 (L_3+3 eV) excitation. All measurements were taken at room temperature. The spectra are shown as measured. No smoothing or other aesthetical interventions were made. The samples were provided by the University of Köln and the University of Oxford for LCO and LSCO, respectively.[12] In RIXS the samples were cleaved in air, while in photoemission they were cleaved in vacuum (2×10^{-10} mbar).

A comprehensive selection of the experimental results in the Cu L_3 peak region is given in Fig. 2. The zero of energy is taken at the peak maximum ($h\nu_{in}$=931.0 eV). The RIXS and RXPS spectra are normalized to the same peak amplitude to better show the evolution of their shape. The RIXS spectra are plotted as a function of the energy transferred to the system in the scattering process ($h\nu_{in}-h\nu_{out}$), and the RXPS results are plotted vs the binding energy (BE). Each spectrum has a vertical offset proportional to the increase of the incident photon energy. In these representations, the non-Raman contributions appear to shift linearly toward the left

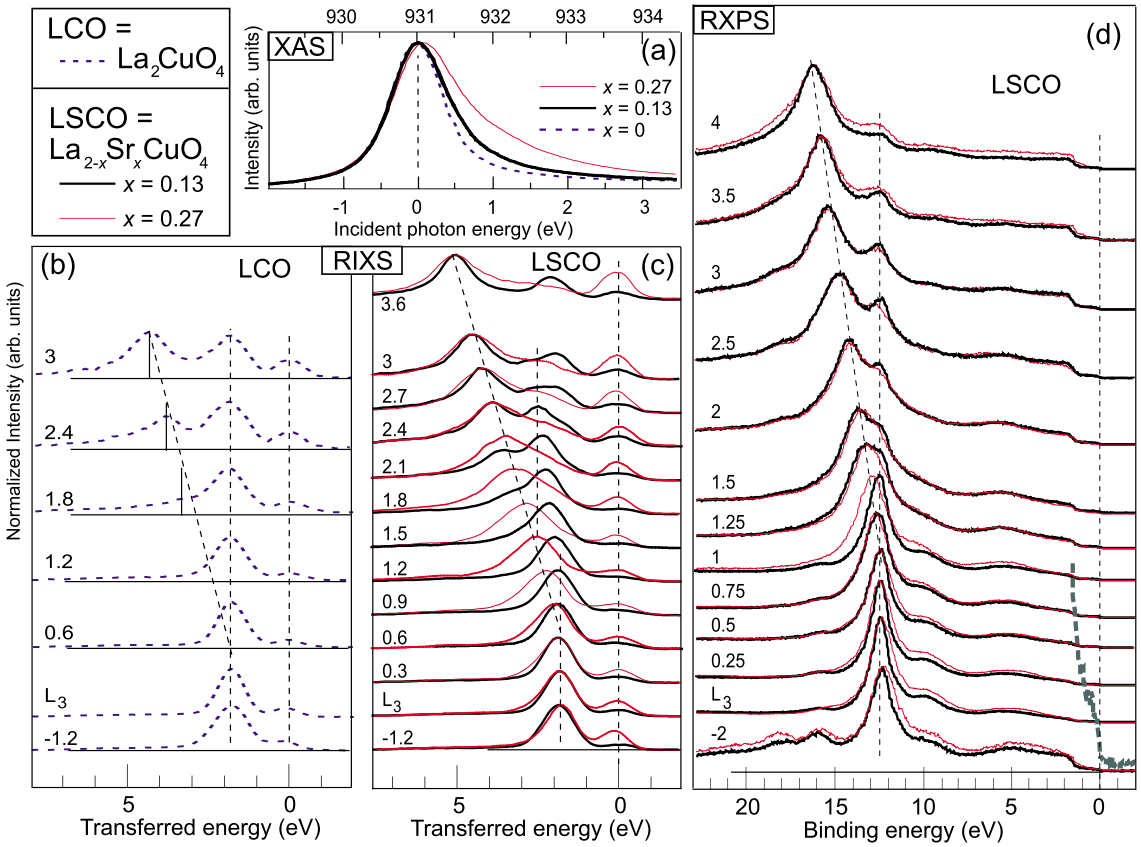

FIG. 2. (Color online) An overview of all experimental results. In all cases, the spectra are normalized to the intensity of the main peak visible in the given energy range. (a) Cu L_3 absorption spectra of LCO and LSCO. (b) RIXS measurements of LCO. (c) RIXS measurements of LSCO samples. (d) RXPS measurements of LSCO (the expanded green spectrum shows the Fermi level cut).

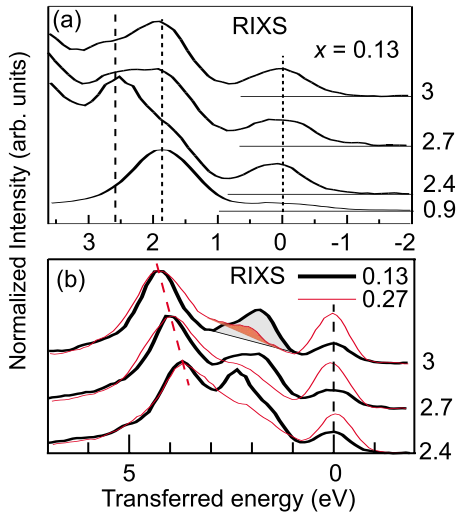

FIG. 3. (Color online) (a) An expansion of RIXS spectra of LSCO with x=0.13). (b) An expansion of the comparison between two dopings in RIXS.

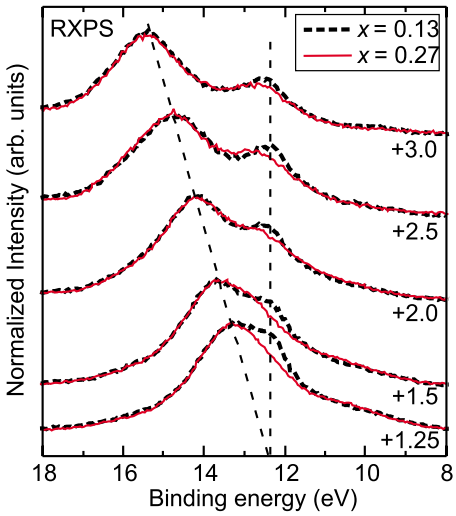

FIG. 4. (Color online) Comparison, for the two doped LSCO samples, of the RXPS spectra excited above the main L_3 peak. The spectra are normalized to the same intensity at an 8 eV binding energy, different from Fig. 2. The x=0.27 sample gives a clearly lower Raman peak with respect to the x=0.13 one, whereas the peak positions are identical in the two samples (above L_3+1.5 eV, where the peak can be distinguished).

when increasing $h\nu_{in}$; those components are highlighted by the inclined dashed straight lines.

The experimental results show that the x-ray absorption spectrum (XAS) L_3 peak has a tail extending at higher binding energies up to 2.5–3 eV, whose intensity increases with doping in agreement with Ref. 13. The RIXS spectral function depends strongly on the doping, whereas RXPS seems much less influenced. The RIXS spectra excited below L_3, at L_3, and up to L_3+0.3 eV are very similar in the three samples and do not change with $h\nu_{in}$. On the contrary, when exciting in the $(L_3+1.5)-(L_3+3)$ eV energy interval, the spectra differentiate themselves very clearly. In particular, for x=0.13, we can recognize two distinct contributions to the *dd* excitation spectrum [see Fig. 3(a)]: Up to L_3+0.9 eV a peak at 1.9 eV dominates, whereas around L_3+2.4 eV a peak at 2.6 eV resonates. The 2.6 eV loss is present also for x =0.27, although weaker and broader, as shown in Fig. 3(b), but it is absent for LCO [see Fig. 2(b)]. Conversely, the peak position of the non-Raman components is the same for all the dopings in both techniques. Following the inclined dashed lines in Figs. 1(b)–1(d), we find that they cross the vertical lines of the main Raman features approximately at the same excitation energy of $\simeq L_3$+0.5 eV. This indicates that the final state energies of the main fluorescence and Auger peaks are little influenced by the doping. Finally, it must be noted that for $h\nu_{in} \geqslant L_3$+1 eV, the non-Raman/Raman intensity ratio increases considerably with x in RIXS, but it shows little dependence on doping in RXPS, as highlighted by the comparison of Figs. 3(b) and 4.

III. CLUSTER MODEL: LOCAL AND NONLOCAL SCREENING

To give a consistent interpretation of the experimental results, we will use the cluster model already successfully used many times for resonant spectroscopies of cuprates,[14] although we will not calculate here any quantitative results based on that model. We will show below that a key role is played by the core hole screening in the intermediate state: Both local and nonlocal screening mechanisms have to be considered.[15] The meaningful electronic states are those of one CuO_6 cluster (tetragonally distorted octahedral structure). In particular, we refer to the 3*d* population of the central Cu ion and to that of the surrounding oxygens. The ground state is then $3d^9$ for LCO, meaning that copper is nominally divalent and all the oxygen 2*p* states are occupied, so that only one hole resides on the cluster. When doping with holes by substituting an x fraction of La atoms with Sr, some of the clusters form Zhang-Rice singlets:[16] Two holes, both with (x^2-y^2) symmetry, reside on the cluster, one mainly with a Cu 3*d* character and one mainly with an O 2*p* character. This corresponds to a $3d^9\underline{L}$ configuration, where $\underline{L}$ indicates a hole mainly with an O 2*p* character. The Cu L_3 resonant XAS main processes are thus $3d^9 \rightarrow \underline{c}3d^{10}$ and $3d^9\underline{L} \rightarrow \underline{c}3d^{10}\underline{L}$ for the undoped and doped sites, respectively, where $\underline{c}$ indicates a Cu 2*p* core hole. The two processes require photons of different energies,[13,17–20] so that the main L_3 peak at 931.0 eV is assigned to the absorption by an undoped site and the tail around 932.5 eV to the absorption by a doped site.

This picture is not sufficient to give a consistent interpretation of our results. So, in analogy to what was suggested by Mizokawa *et al.* in Ref. 20, we introduce a third type of states reachable in the XAS process. We indicate by $\underline{c}3d^{10}S$ a "nonlocally screened" (or "well screened") state reached when the absorption process involves more than one cluster and the energy carried by the absorbed photon is partly transferred to the neighboring clusters. In the XAS final state, the core hole acts as a strong positive extra charge located on the central Cu, and it attracts an extra electron into the 3*d* shell (core hole screening). When the core hole screening is ac-

complished by attracting an electron from outside the cluster, one electron is added to the cluster, resulting in a more effective screening. So, for a given doped site, the energy of the unscreened $\underline{c}3d^{10}\underline{L}$ final state is expected to be higher than that of the screened $\underline{c}3d^{10}S$ one. Somehow different is the case of an undoped site, where the screening cannot be made by the addition of an extra electron to the already full $3d$ shell. We can expect though that $\underline{c}3d^{10}S$ of a doped site and $\underline{c}3d^{10}$ of an undoped site have comparable energies, both lower than that of $\underline{c}3d^{10}\underline{L}$. This fact was shown in Ref. 20 for $LaCuO_3$: Despite a nominally pure $3d^9\underline{L}$ ground state, two separate peaks are found in the absorption spectrum, corresponding to the screened and unscreened XAS final states. The nonlocal screening is favored by the intercluster interaction, which is weak in $NaCuO_2$ (giving almost no $\underline{c}3d^{10}S$ peak),[18] medium in $LaCuO_3$ (two peaks of comparable intensity),[20] and strong in LSCO (weak unscreened peak). The interpretation of the RIXS and RXPS spectra has thus to take into account three possible intermediate states: $\underline{c}3d^{10}$ for undoped sites, and $\underline{c}3d^{10}S$ and $\underline{c}3d^{10}\underline{L}$ for the doped sites, keeping in mind that $\underline{c}3d^{10}$ and $\underline{c}3d^{10}S$ can be very close in energy.

The XAS final states coincide with the intermediate states of both RIXS and RXPS, and the incident photon energy can be used to choose them. On the contrary, the two techniques differ in the final states: RIXS is charge neutral; RXPS is electron removal. We concentrate here on subsets of final states of both types. In RIXS, we ignore the charge transfer excitations (usually broad and of energy higher than 2 eV in cuprates), and we analyze the behavior of *dd* excitations, which differ from the ground state only in the way the $3d$ orbitals are populated. *dd* excitations give a clear peak at around 1.8–2.6 eV transferred energy. In RXPS, we focus on the main peak at around 12.5 eV binding energy that corresponds to a $3d^8(^1G)$ final state, whereas we disregard the featureless lower binding energy region dominated by $3d^9\underline{L}$ configurations.[22,21] In Fig. 5(a), we present the general mechanism giving rise to the Raman features both in RIXS and RXPS. As we are dealing with a second order process governed by the Kramers-Heisenberg formula,[23] the scattering process brings the system (our cluster) from the ground to the final state via a given intermediate state ($|g\rangle \rightarrow |m\rangle \rightarrow |f\rangle$), and $\Delta E = h\nu_{in} - E_{out}$ is constant and equal to the energy difference between $|f\rangle$ and $|g\rangle$. On the contrary, when the scattering is made via a delocalized intermediate state ($|g\rangle \rightarrow |m'\rangle \rightarrow |f'\rangle$), we have the non-Raman behavior sketched in Fig. 5(b), where E_{out} is constant because the excess energy carried by the incident photon is lost outside the scattering cluster whose energy we are considering.[6,24]

IV. DISCUSSION: RAMAN AND NON-RAMAN FEATURES IN RESONANT INELASTIC X-RAY SCATTERING AND RESONANT X-RAY PHOTOEMISSION SPECTROSCOPY

Within our model, we can describe the scattering mechanisms taking place at doped and undoped sites. At an undoped site, starting from a $3d^9$ ground state, the Raman features of RIXS and RXPS reached via the $\underline{c}3d^{10}$ intermediate

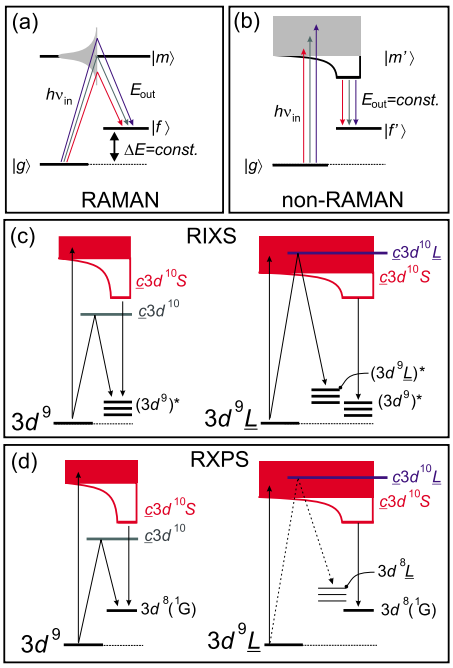

FIG. 5. (Color online) [(a) and (b)] The conventional schematic representation of a resonant inelastic process leading to Raman (a) and non-Raman (b) behaviors of the spectral features. [(c) and (d)] The schematic representation of RIXS (c) and RXPS (d) at an undoped (left) and hole doped site (right). The line of the transition to the $3d^8\underline{L}$ set of final states is dashed to indicate that this path is not considered in our discussion because it does not give a sharp peak in RXPS.

state (931.0 eV) correspond to $(3d^9)^*$ and $3d^8(^1G)$ final states, respectively (the * indicates *dd* excitations) [see left schemes in Figs. 4(c) and 4(d)]. When exciting well above L_3, the same final states are reached via the $\underline{c}3d^{10}S$ intermediate state, giving non-Raman features. It is important to note that when exciting well above L_3, the intermediate state *is not* $\underline{c}3d^9$, as one could naively expect from an electron possessing an extra energy with respect to the resonance. In fact, we know from photoemission that in CuO and LCO (undoped cuprates) the dominant final state of $2p$ photoemission has a $\underline{c}3d^{10}$ character (main peak, around 933 eV binding energy), whereas the $\underline{c}3d^9$ final state gives rise to the satellite at 7 eV greater BE.[14] Moreover the main $2p$ XPS peak is influenced both by local and nonlocal core hole screening: van Veenendaal has recently shown that the nonlocal character $\underline{c}3d^{10}S$ dominates in undoped sites.[25] Here, we confirm that assignment also for XAS of undoped materials above L_3: The intermediate state of RIXS and RXPS is mainly $\underline{c}3d^{10}S$ and not $\underline{c}3d^9$ nor $\underline{c}3d^{10}\underline{L}$. In fact, in RXPS, the locally screened $\underline{c}3d^{10}\underline{L}$ intermediate state would lead to a $3d^8\underline{L}$ final state that is different from the $3d^8(^1G)$ that gives the strong peak we are actually observing.

The situation at a doped site is similar, but with important differences: The Raman features can arise only via the $\underline{c}3d^{10}\underline{L}$ intermediate state, whereas the non-Raman ones are the same as in the undoped sites because they are reached via the nonlocally screened $\underline{c}3d^{10}S$ intermediate state [see the schemes on the right side in Figs. 4(c) and 4(d)]. We can thus

understand the different behaviors of the two techniques. When going through the localized intermediate state $\underline{c}3d^{10}\underline{L}$, the $(3d^9\underline{L})^*$ set of final states can be effectively reached in RIXS, but the $3d^8(^1G)$ state is inaccessible via a Raman process in RXPS.[26] This explains why the non-Raman/Raman ratio is very sensitive to the doping in RIXS and much less in RXPS. In a doped LSCO sample, when exciting above L_3, the RXPS Raman signal is given by the undoped sites excited on the Lorentzian tail of the main L_3 peak and the non-Raman component is given by the doped sites via the well screened $\underline{c}3d^{10}S$ intermediate state. So, changing the doping from $x=0.13$ to $x=0.27$ leads to a decrease of the RXPS Raman spectral weight of the order of 20%–30%, rather constant at all excitation energies above the L_3 absorption edge. This is exactly what we observe in Fig. 4: Above $L_3+1.25$ eV, the non-Raman/Raman intensity ratio is rather constant for both LSCO samples, and the $\underline{c}3d^{10}\underline{L}$ resonance does not affect that ratio. On the contrary, in RIXS, a second Raman channel becomes accessible around $L_3+2.4$ eV (see Fig. 3). The Raman peak changes shape because it corresponds to the *dd* excitations of the doped sites $[(3d^9\underline{L})^*$ final states], characterized by two particles on the cluster instead of one. The average excitation energy is higher (2.6 eV instead of 1.9 eV) due to the Coulomb and exchange interactions between the two holes, interactions that are absent in the one hole case $[(3d^9)^*$ final states of undoped sites].

To further support our assignment, we can look at the literature on RXPS of cuprates where the $3d^8(^1G)$ peak had already been monitored. Its BE, when exciting at the L_3 peak, varies by less than 0.7 eV in various cuprate samples with divalent Cu, rather independently of the doping [LSCO gives 12.4–13.1 eV,[27] CuO gives 12.5 eV,[22] the BiSrCaCuO family gives 12.3 eV,[21,28] and $LaCuO_3$ gives 12.5 eV (Ref. 20)], whereas it is very different for a lower valence [Cu metal gives 14.2 eV, (Ref. 6) and Cu_2O gives 15.1 eV (Ref. 22)]. Moreover, the spin resolved resonant photoemission data demonstrate that the peak around 12.5 eV always has a pure singlet character.[27] These facts demonstrate that the main peak in RXPS is insensitive to the doping in divalent Cu sites because it corresponds to a very atomic ^1G final state always reached through a $\underline{c}3d^{10}$ intermediate state, be it localized (in the undoped samples) or delocalized (in the doped samples).

We can finally summarize the interpretation of all our experimental observations. The Raman RIXS features are of one type only in LCO because they always correspond to the $(3d^9)^*dd$ excitation spectrum for all excitation energies. In LSCO with $x=0.13$, they change shape above L_3+2 eV, where they correspond to $(3d^9\underline{L})^*dd$ excitations: The Coulomb repulsion and the magnetic interaction of the two holes increase the average excitation energy from 1.9 to 2.6 eV.[29] As far as the spectroscopic assignment is concerned, we have already shown in Ref. 7 that the main Raman feature in the undoped system is an unresolved doublet of *dd* excitations with similar contributions from the xy and $[xz,yz]$ final state symmetry (z along the c axis). Even if the present experiment cannot better resolve the *dd* excitations in undoped sites, it shows anyway that in optimally doped LSCO the RIXS can clearly disentangle *dd* excitations of doped and undoped sites. It will be interesting in the future to study with greater resolution the two hole excitation spectrum. The Raman RXPS peak always corresponds to the $3d^8(^1G)$ final state, independently of the excitation energy. The unscreened $\underline{c}3d^{10}\underline{L}$ intermediate state cannot lead to that final state.

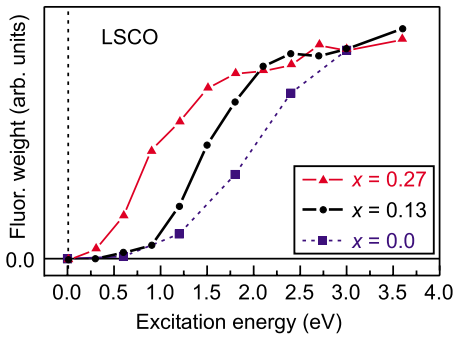

FIG. 6. (Color online) The experimental relative spectral weight of the non-Raman component in RIXS plotted as function of the incident photon energy for the three LSCO samples.

The non-Raman features are always attributed to final states reached via the same well screened $\underline{c}3d^{10}S$ intermediate state, both in RIXS and RXPS. This explains why the emission energy is constant vs $h\nu_{in}$ and vs x. What changes is the excitation energy threshold, giving access to the nonlocally screened intermediate state. As the $\underline{c}3d^{10}S$ intermediate state is delocalized, the energy conservation law cannot be applied to the cluster, and the entire solid comes into play. That is why in Fig. 5, the nonlocally screened state is indicated as a red shaded band plus a bottom level that determines the emission energy. The access to the band in the excitation step is influenced by the doping; the energy of the bottom level is little or not influenced by the doping. A more traditional way of describing the situation would be to invoke some kind of relaxation process in the intermediate state, bringing it to the bottom level before the main deexcitation step. This picture would imply a loss of coherence in the second order processes (RIXS or RXPS), which is not necessary to account for the experimental observations. On the contrary, some other experiments in RIXS (magnetic circular dichroism in the perpendicular geometry) have demonstrated that even in metallic samples, where the non-Raman component hugely dominates the spectra, the magnetic effects at the L_3 resonance can be explained only in a second order process model.[30,31] Here, we do not pretend to exclude that some kind of (incoherent) relaxation process take place in the intermediate state, although we are highlighting that invoking a relaxation is not necessary to explain the non-Raman behavior of RXPS and RIXS features.

Our experiments can provide us the threshold of the nonlocally screened states. For a quantitative assessment, we have used the RIXS spectra only because we have the data for the three dopings and because it is easier to separate the non-Raman and Raman components. In Fig. 6, we show the relative spectral weight of the non-Raman component over the total intensity. Due to the intrinsic uncertainties in the data treatment, the results should be treated with caution. Nevertheless, Fig. 6 indicates very clearly that in the un-

doped sample the screening process becomes effective only 2 eV above L_3, i.e, around 933.0 eV. In the doped samples, the threshold is 0.5 and 1 eV lower than in LCO for $x=0.13$ and $x=0.27$, respectively. The presence of doped sites in the CuO_2 planes increases the intercluster interaction and the band formation. We underline here that the results of Fig. 6 concern the intermediate state, not the ground or final states. But it is important for RIXS anyhow. In fact, from Fig. 3, we can observe that going from $x=0.13$ to $x=0.27$ does not help in better studying with RIXS the *dd* excitations of doped sites. This is because the $\underline{c}3d^{10}\underline{L}$ intermediate state suffers from a too strong concurrence of the delocalized intermediate state. This finding seems somehow related to the density of carriers in the conduction planes.

Aside from the cluster model interpretation, we can compare our results to more traditional spectroscopies. In LCO, the onset of the non-Raman peak along the $h\nu_{in}$ scale correlates rather well with the results of reflectivity and photoconductivity data,[32–34] which show that optical absorption above ~ 2 eV gives charged excitations contributing to the conductivity. It is thus quite natural to assign the onset of the non-Raman contribution to an intermediate state having the hot electron (created by absorption) hopping and bringing away the excess energy, so that the emission spectrum is independent of $h\nu_{in}$. Moreover, when the system is doped, it becomes metallic, allowing many more channels for losing the excess energy in the intermediate state due to the greater mobility of charge carriers.[35] Our findings of Fig. 6 are thus reasonable: In RIXS, the threshold of the non-Raman contribution is at lower $h\nu_{in}$ when increasing x and its relative intensity at a given $h\nu_{in}$ grows with x.

V. CONCLUSIONS

In conclusion, we have identified the *dd* excitations of both doped and undoped sites in LSCO: The two hole excited states have a spectral distribution extending up to 2.6 eV from the Zhang-Rice singlet ground state, to be compared to the 1.9 eV average *dd* excitation energy of undoped sites. Moreover, we have found that RIXS is much more sensitive to the hole doping level than valence band resonant photoemission. At the doped sites, the RXPS Raman feature is suppressed, leading to a diminished sensitivity to the doping level. The different final states of RIXS and RXPS act as intermediate state selectors. The comparison of RIXS and RXPS has been essential for demonstrating that the nonlocal core hole screening plays a crucial role in the intermediate state determining the onset of the non-Raman features in the RIXS and RXPS spectra. We have found that the nonlocal screening is more effective with increased hole doping, i.e., in more metallic samples, because it has a lower onset. This picture will also help in the interpretation of RIXS and RXPS spectra of strongly correlated systems, other than cuprates.

[1] A. Kotani and S. Shin, Rev. Mod. Phys. **73**, 203 (2001).
[2] A. Kotani, Eur. Phys. J. B **47**, 3 (2005).
[3] T. Åberg and B. Craseman, in *Resonant Anomalous X-Ray Scattering*, edited by G. Materlik, C. Sparks, and K. Fischer (North-Holland, Amsterdam, 1994).
[4] M. Finazzi, N. B. Brookes, and F. M. F. de Groot, Phys. Rev. B **59**, 9933 (1999).
[5] M. Finazzi, G. Ghiringhelli, O. Tjernberg, P. Ohresser, and N. B. Brookes, Phys. Rev. B **61**, 4629 (2000).
[6] A. Föhlisch, O. Karis, M. Weinelt, J. Hasselström, A. Nilsson, and N. Mårtensson, Phys. Rev. Lett. **88**, 027601 (2002).
[7] G. Ghiringhelli, N. B. Brookes, E. Annese, H. Berger, C. Dallera, M. Grioni, L. Perfetti, A. Tagliaferri, and L. Braicovich, Phys. Rev. Lett. **92**, 117406 (2004).
[8] A. Damascelli, Z. Hussain, and Z.-X. Shen, Rev. Mod. Phys. **75**, 473 (2003).
[9] E. Dagotto, Rev. Mod. Phys. **66**, 763 (1994).
[10] C. Dallera, E. Puppin, A. Fasana, G. Trezzi, N. Incorvaia, L. Braicovich, N. B. Brookes, and J. B. Goedkoop, J. Synchrotron Radiat. **3**, 231 (1996).
[11] G. Ghiringhelli, A. Tagliaferri, L. Braicovich, and N. B. Brookes, Rev. Sci. Instrum. **69**, 1610 (1998).
[12] The LSCO samples were provided by the National Crystal Growth Facility for Superconducting Oxide Crystals, Clarendon Laboratory, Department of Physics, University of Oxford, UK.
[13] C. T. Chen, L. H. Tjeng, J. Kwo, H. L. Kao, P. Rudolf, F. Sette, and R. M. Fleming, Phys. Rev. Lett. **68**, 2543 (1992).
[14] Z.-X. Shen, J. W. Allen, J. J. Yeh, J.-S. Kang, W. Ellis, W. Spicer, I. Lindau, M. B. Maple, Y. D. Dalichaouch, M. S. Torikachvili, J. Z. Sun, and T. H. Geballe, Phys. Rev. B **36**, 8414 (1987).
[15] M. A. van Veenendaal and G. A. Sawatzky, Phys. Rev. Lett. **70**, 2459 (1993).
[16] F. C. Zhang and T. M. Rice, Phys. Rev. B **41**, 7243 (1990).
[17] J. Fink, N. Nucker, E. Pellegrin, H. Romberg, M. Alexander, and M. Knupfer, J. Electron Spectrosc. Relat. Phenom. **66**, 395 (1994).
[18] D. D. Sarma, O. Strebel, C. T. Simmons, U. Neukirch, G. Kaindl, R. Hoppe, and H. P. Müller, Phys. Rev. B **37**, 9784 (1988).
[19] M. A. van Veenendaal and G. A. Sawatzky, Phys. Rev. B **49**, 3473 (1994).
[20] T. Mizokawa, T. Konishi, A. Fujimori, Z. Hiroi, M. Takano, and Y. Takeda, J. Electron Spectrosc. Relat. Phenom. **92**, 97 (1998).
[21] L. H. Tjeng, C. T. Chen, and S.-W. Cheong, Phys. Rev. B **45**, 8205 (1992).
[22] L. H. Tjeng, C. T. Chen, J. Ghijsen, P. Rudolf, and F. Sette, Phys. Rev. Lett. **67**, 501 (1991).
[23] M. van Veenendaal, P. Carra, and B. T. Thole, Phys. Rev. B **54**, 16010 (1996).
[24] L. Braicovich, C. Dallera, G. Ghiringhelli, and N. B. Brookes, Solid State Commun. **102**, 709 (1997).
[25] M. A. van Veenendaal, Phys. Rev. B **74**, 085118 (2006).
[26] Other RXPS final states are still reachable via a Raman process leading to a variety of configurations ($3d^8\underline{L}, 3d^9\underline{L}^2$), but they do not correspond to the sharp $3d^8(^1G)$ peak we are using in our discussion.
[27] N. B. Brookes and G. Ghiringhelli (unpublished).

[28] M. Qvarford, J. F. van Acker, J. N. Andersen, R. Nyholm, I. Lindau, G. Chiaia, E. Lundgren, S. Söderholm, U. O. Karlsson, S. A. Flodström, and L. Leonyuk, Phys. Rev. B **51**, 410 (1995).
[29] In the present work, we did a more accurate energy calibration with respect to Ref. 7; minor differences in the energies of the spectral features do not change the message of Ref. 7.
[30] L. Braicovich, G. van der Laan, G. Ghiringhelli, A. Tagliaferri, M. A. van Veenendaal, N. B. Brookes, M. M. Chervinskii, C. Dallera, B. De Michelis, and H. A. Dürr, Phys. Rev. Lett. **82**, 1566 (1999).
[31] L. Braicovich, G. Ghiringhelli, A. Tagliaferri, G. van der Laan, E. Annese, and N. B. Brookes, Phys. Rev. Lett. **95**, 267402 (2005).
[32] J. P. Falck, A. Levy, M. A. Kastner, and R. J. Birgeneau, Phys. Rev. Lett. **69**, 1109 (1992).
[33] T. Thio, R. J. Birgeneau, A. Cassanho, and M. A. Kastner, Phys. Rev. B **42**, 10800 (1990).
[34] M. A. Kastner, R. J. Birgeneau, G. Shirane, and Y. Endoh, Rev. Mod. Phys. **70**, 897 (1998).
[35] A. Ino, C. Kim, N. Nakamura, T. Yoshida, T. Mizokawa, A. Fujimori, Z.-X. Shen, T. Kakeshita, H. Eisaki, and S. Uchida, Phys. Rev. B **65**, 094504 (2002).